

Automated tuning of double quantum dots into specific charge states using neural networks

R. Durrer,¹ B. Kratochwil,¹ J. V. Koski,¹ A. J. Landig,¹ C. Reichl,¹ W. Wegscheider,¹ T. Ihn,¹ and E. Greplova^{2,*}

¹*Department of Physics, ETH Zürich, Otto-Stern-Weg 1, CH-8093 Zürich, Switzerland*

²*Department of Physics, ETH Zürich, Wolfgang-Pauli-Str. 27, CH-8093 Zürich, Switzerland*

While quantum dots are at the forefront of quantum device technology, tuning multi-dot systems requires a lengthy experimental process as multiple parameters need to be accurately controlled. This process becomes increasingly time-consuming and difficult to perform manually as the devices become more complex and the number of tuning parameters grows. In this work, we present a crucial step towards automated tuning of quantum dot qubits. We introduce an algorithm driven by machine learning that uses a small number of coarse-grained measurements as its input and tunes the quantum dot system into a pre-selected charge state. We train and test our algorithm on a GaAs double quantum dot device and we consistently arrive at the desired state or its immediate neighborhood.

I. INTRODUCTION

Engineered quantum devices are currently at the forefront of scientific research [1–3]. The enormous progress in the precision of the engineering and control of these devices at the level of individual particles or excitations allows researchers to build quantum coherent devices such as qubits which are the building blocks of quantum information processing architectures. Such devices have been successfully built utilizing different platforms such as NV-centers [4, 5], superconducting qubits [6, 7], thin nanomaterials [8] and nanowires [9, 10], to name just a few.

Extrapolating the success of semiconductor technology and its scaling properties from the past into the future, qubits based on gate defined semiconductor quantum dots (QDs) are seen as promising candidates for scalable quantum computing. Experiments have successfully demonstrated long coherence times [11], fast gate operations [12, 13] and long-distance qubit coupling [14–17]. However, to change the number of electrons/holes in the QDs and to tune the coupling to neighbouring QDs and reservoirs, an operator has to change the corresponding voltages applied to the gate electrodes. The relation between applied gate voltages and the physical parameters to be tuned is highly device specific and, thus, requires calibration measurements. Automating the tuning process is therefore one of the key challenges in making semiconductor architectures scalable.

Progress in characterizing, controlling and tuning complex quantum systems has been achieved through a variety of algorithmic methods [18–21]. Applying machine learning techniques for parameter estimation and tuning of quantum systems has been a promising avenue within this endeavor [22–27]. Machine learning methods can be used to automate tasks previously done by humans [28] and construct high-quality abstract models interpreting complex measurements. They are

fast to evaluate even without implementing a device- or system-specific physical model, which can be complex and lengthy to simulate in the case of QD qubits.

In this work we present a stepping stone towards automated QD tuning. Our algorithm automatically tunes a double quantum dot (DQD) initially in an unknown charge state into a pre-defined charge state. This is relevant as different qubit implementations require a well-defined number of electrons in each QD, such as for the hybrid qubit [29, 30], the resonant exchange qubit [31, 32], or the quadrupolar exchange-only qubit [33]. We employ convolutional neural networks to recognize transitions between charge states in the charge stability diagram. We test our method by training and testing it experimentally with two DQD devices based on a GaAs heterostructure, and we evaluate its performance.

II. EXPERIMENTAL SETUP

A scanning electron micrograph of our device, that is capable of forming up to three QDs, is shown in Fig.1. The device has a two-dimensional electron gas 90 nm below the surface, embedded into a GaAs/AlGaAs heterostructure. We confine electrons by applying negative voltages to gold gates on top of the heterostructure. The design permits the formation of up to three QDs (labeled QD1, QD2 and QD3) in a linear array. This allows us to realize two different DQD devices, formed either by QD1 and QD2 (DQD1), or by QD2 and QD3 (DQD2). Whenever we form a DQD the remaining QD is not formed and is therefore part of the reservoir. Three finger gates, visible at the bottom of Fig.1, are used individually to define a quantum point contact (QPC) measuring charge transitions in the nearby QDs. When we measure charge transitions of DQD1 (DQD2) we chose the middle (right) gate as the QPC gate and keep the remaining two gates grounded.

Fig. 2 shows a charge stability diagram of DQD1. We plot the change $\partial I_{\text{QPC}}/\partial V_{\text{PG}}$ of the current I_{QPC} in the quantum point contact as a function of the plunger

* geliska@phys.ethz.ch

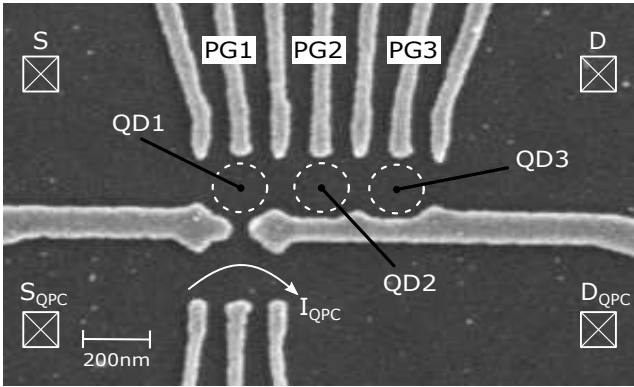


FIG. 1. Scanning electron microscope image of the GaAs/AlGaAs sample. The dashed circles indicate the positions of the three QDs that can be formed. The crossed boxes indicate ohmic contacts.

gate voltages V_{PG1} and V_{PG2} . A change of the electron number in either of the dots causes a sharp peak in $\partial I_{QPC}/\partial V_{PG}$, seen as tilted lines in Fig. 2. The slopes, intensities and separations of these lines, called charge transition lines, are not precisely reproducible with present day technologies in nominally identical devices and are therefore device-specific. Thus, charge stability diagrams of distinct devices may look different. Furthermore, the properties of the charge stability diagrams may vary for different gate voltages using the same device. This diversity of charge stability diagrams makes manual tuning of such quantum devices a matter of human supervision, where the experience of the operator influences the efficiency of the process.

We label the charge states as (n,m) with n and m being the number of electrons in QD1 and QD2, respectively. We assign the charge states to plaquettes of the charge stability diagram by counting the number of charge transition lines starting from the $(0,0)$ state as illustrated in Fig. 2.

A scheme for the efficient measurement of the charge stability diagram driven by machine learning has been introduced in Ref. 22. Automated tuning to a specific QD regime (single or DQD) has been recently achieved in Refs. 26 and 34. Our algorithms complement these achievements and could be combined with some of them. The starting point for the procedures developed here is any gate voltage setting, where a DQD in the Coulomb-blockade is well-defined, with unknown and arbitrary charge state. The problem we attempt to solve is then stated as: Given a DQD in an unknown initial charge configuration (n_i, m_i) , find a plunger gate voltage configuration for which the charge configuration is equal to the pre-selected charge state (n_f, m_f) required for operating the qubit.

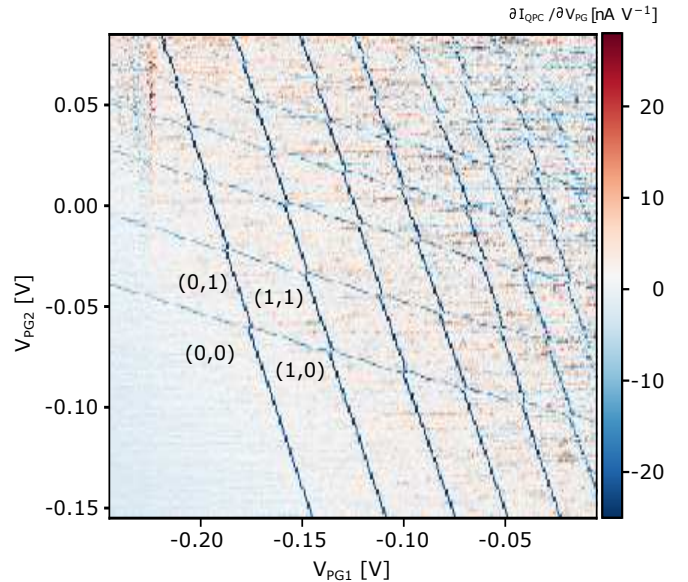


FIG. 2. Charge stability diagram of the DQD based on QD1 and QD2 from the sample in Fig. 1. The charge occupation is indicated as (n,m) where n denotes the number of electrons on QD1 and m the number of electrons on QD2.

III. ALGORITHM

We split the task of finding the required charge configuration into two steps. Starting from (n_i, m_i) the first step is to find a plunger gate voltage configuration for which the DQD is completely empty [charge state $(0,0)$]. In the second step, the algorithm loads electrons onto the QDs until the desired charge occupation (n_f, m_f) is reached. For each of the two steps we use a convolutional neural network trained to recognize charge transition lines in the charge stability diagram. A detailed discussion of the machine learning models used is provided in section IV.

As illustrated in Fig. 3 (a), we find the $(0,0)$ charge configuration by measuring a small rectangular patches of the charge stability diagram with low resolution. If the algorithm identifies any charge transition lines it decreases both plunger gate voltages. This process is repeated until no charge transition lines are recognized by the convolutional neural network. Compared to the measurement shown in Fig. 2 (resolution 1mV, 241×241 points) the patches are low resolution (resolution 6 - 9 mV) and small size (20×20 points), and thus fast to measure. However, the size of these patches is chosen at least twice as large as the largest line spacing between two consecutive charge transition lines to ensure that no line is missed. We can determine the patch size experimentally by one dimensional plunger gate sweeps or estimate it from the geometric capacitance between the gate and the dots [35]. We refer to the plunger gate voltage configuration, for which the algorithm determines the DQD to be empty, as the “reference point”. This reference point

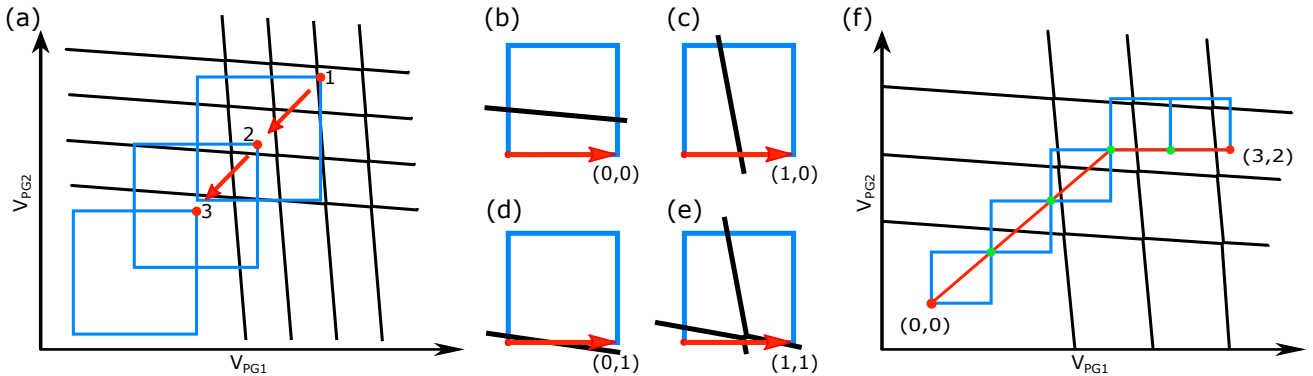


FIG. 3. (a) Schematic illustration of the algorithm finding a charge reference point. The black lines indicate charge transition lines, the blue boxes are the patches used for the classification with the neural network. The red dot at the top right corner of a patch corresponds to the point in the charge stability diagram for which the charge occupation is assessed. (b)-(e) Schematics of the patches for the second neural network in blue and charge transition lines in black. The red arrows indicate a path segment. Along each of the indicated path segments a different charge transition occurs indicated as (n, m) at the end of the arrows. (f) An illustration of a path (red line) connecting the $(0,0)$ charge regime with the $(3,2)$ charge regime. The path constitutes of five path segments belonging to the patches in blue. The algorithm chooses the diagonal path when the electron number in both dots needs to be increased. As soon as the final occupation on the second dot is reached only horizontal path segments are used to only load electrons on QD1.

is the starting point for the second step of the tuning algorithm.

In the second step, we tune from the reference point to the desired charge state (n_f, m_f) . We do this by again measuring rectangular patches of the charge stability diagram and subsequently classifying them using another convolutional neural network. However, the patches are now 28×28 measurement points with a finer resolution (of 1 mV). Their size is chosen such that at most one charge transition per QD occurs in-between any two corners of the patch. The convolutional network is trained to recognize charge transitions occurring between the lower left corner of the patch and the remaining corners. The four different classification outcomes of this step are illustrated in Figs. 3 (b) - (e). We place the lower left corner of the first patch at the $(0,0)$ reference point. We then proceed as depicted in Fig. 3 (f). The patches are connected and jointly build a path along which charge transitions are identified. For each corner of the patches, the charge occupation of the DQD is known, and the path consisting of the patches is extended until the pre-selected charge state is found.

IV. MACHINE LEARNING MODELS

We use two different neural network-based models for the two steps described above, namely to (a) find the zero charge reference point $(0,0)$ and (b) determine the path in the parameter space of plunger gate voltages towards the pre-selected charge configuration (n_f, m_f) . Both models are trained to recognize the charge transition lines in the measured patches. The plunger gate voltages are then adjusted based on the presence and direction of the charge transition lines.

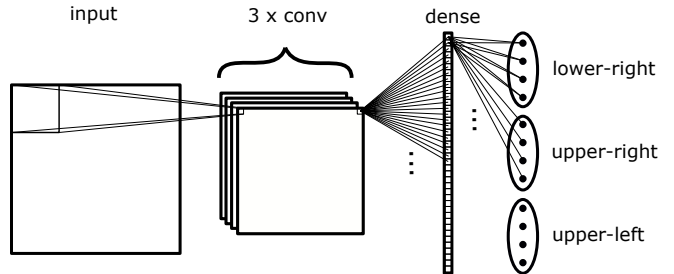


FIG. 4. Architecture of the convolutional neural network that recognizes charge transitions between the corners of a given input frame. The neural network consists of three convolutional layers, one dense layer and three outputs with four classification outcomes each.

The convolutional neural network for the first step of the algorithm, responsible for finding the $(0,0)$ state, is trained by supervised learning using coarsely measured patches of 20×20 data points in the charge stability diagram as an input. The output of the network is binary: either both QDs are empty or at least one of them is occupied. In other words, since the patch of the charge stability diagram extends beyond the maximal spacing of two charge transition lines, the network effectively detects if there is a charge transition line for any of the QDs within the patch. The model we use for the first part of the algorithm consists of two convolutional and one dense layer. For the full technical description see Appendix B.

The neural network for the second part of the tuning-algorithm is trained as a classifier that recognizes individual charge transitions. The output of the network is then used to reach an arbitrary final charge state (n_f, m_f) from the state $(0,0)$. The input of this more complex classifier are finer 28×28 patches of the charge

stability diagram. The output contains 12 elements that precisely specify which charge transition has been observed in a given patch. More specifically, the presence of one of the possible charge transition scenarios shown in Fig. 3 (b) - (e) is determined for the lower right, upper right and upper left corner of the patch (see Fig. 4). Apart from this specific structure of the output design, which we chose to fit to the physics of interest, the body of the network has a standard construction with three convolutional layers and one dense layer. For the technical details of the architecture see Appendix B.

We trained both neural networks on experimentally measured data. In particular, we measured 128 (470) complete charge stability diagrams of DQD1 in finer resolution (coarse resolution) and the operator marked each charge transition line for all data sets. We varied the gate voltage configuration for each of the measured charge stability diagrams and fixed the (compensated) plunger gate range. From each charge stability diagram we cut out random patches, and we use a script to automatically translate the marked transition lines into labels for each patch. For the first part of the algorithm, the labels are single binary variables, while for the second part of the algorithm each patch has three labels, i.e. one for each corner, see Fig. 4. To create a richer training set we augment each charge stability diagram by a factor of 18. The augmentation is achieved by various combinations of rotations and axis scaling and allows us to include a larger variety of physical plausible measurement scenarios into our training set. For details see Appendix A. The resulting training sets contain the order of 10^5 patches and both networks are optimized to minimize the error between the labels assigned by the human operator and those assigned by the network. All training data was obtained from DQD1.

V. RESULTS

The neural network developed to find the reference point $(0,0)$ is trained on 650'000 labeled patches. After training the neural network, the model has an accuracy of 98.9% on the evaluation data set. The accuracy score corresponds to the probability that each single patch is classified correctly to represent an empty or an occupied QD. Once the network is able to reliably classify independent patches, we can test the reference point finding part of the algorithm by starting from an arbitrary charge configuration (n_i, m_i) in the DQD and check if the algorithm reaches the correct reference point $(0,0)$. The algorithm succeeded in 144 out of 160 runs, resulting in a success rate of 90%. The neural network used for the second part of the algorithm is trained on 530'000 labeled patches. The accuracy of this neural network, i.e., the probability that the correct charge transition is recognized for any of the corners individually, is found to be 96% on the evaluation data set.

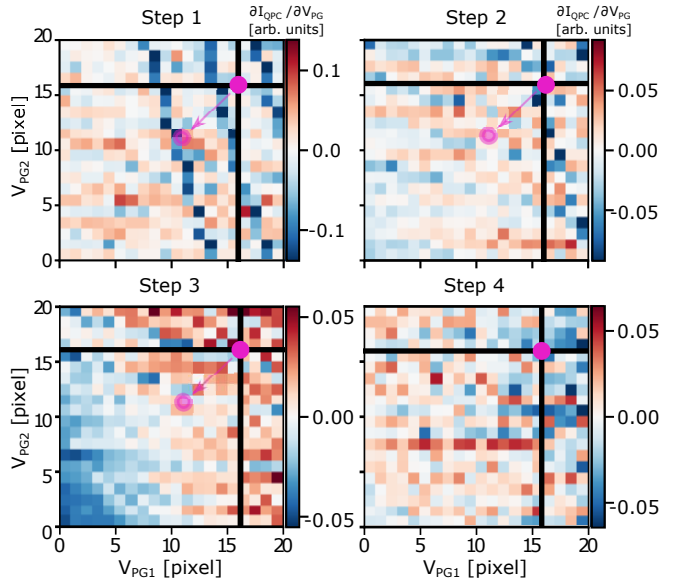


FIG. 5. A successful run of the reference finding algorithm. The solid purple dot indicates the voltage configuration for which the charge occupation of the DQD is assessed. The faint purple dot indicates the voltage configuration for which the charge occupation is assessed in the next step. In Step 1 to Step 3, the DQD is occupied, whereas in Step 4 the DQD is empty and the algorithm terminates.

We test and evaluate the performance of the complete algorithm by first selecting a desired final state (n_f, m_f) . The DQD is then initialized in an arbitrary initial charge state (n_i, m_i) and we run the first part of the algorithm to reach the reference point $(0,0)$. Once the reference point is reached, the second part of the al-

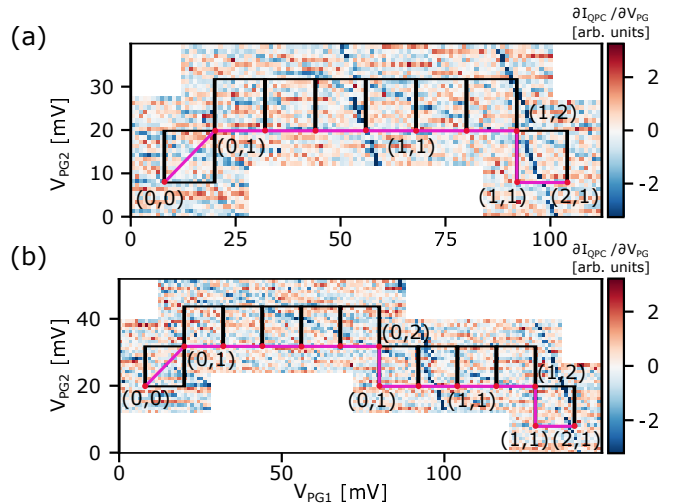


FIG. 6. Two successful runs of the auto-tuner for which the plunger gate voltages for the desired charge occupation is found. The boxes in black denote the patches that linked together, form a path shown in red connecting the $(0,0)$ charge occupation with the desired charge occupation.

gorithm identifies the relevant charge transition lines and tunes the DQD to the selected final state.

Fig. 5 shows a run of the first part of the algorithm that identifies the charge reference point. To make sure not to miss any charge transition lines at the edge of the patch, the evaluation of the dot occupation number is done at the crossing point of the two black lines indicated by a purple dot. If the dot is not yet empty a new patch is measured at the position marked by the arrow. In Step 1 to Step 3 there are charge transition lines within the patch and the algorithm correctly classifies them as occupied. In Step 4, no charge transition lines are present and the patch is correctly classified as empty.

In Fig. 6, we show two paths connecting a reference point to a point in the charge stability diagram with the correct charge state configuration. Both runs are successful and the correct charge regime (2, 1) is found. In black, the charge occupation is indicated after each detected charge transition. Both tuning runs were measured on DQD2 (the system that was not used for training).

The auto-tuner algorithm successfully reached the desired charge configuration in 91 out of 160 conducted test runs, which corresponds to a success rate of 57%. We tested the tuning on both DQD1 and DQD2 and found the score to be independent of the DQD used. This indicates good generalization of the machine learning models across the device. Allowing for a deviation of one electron, the success rate increases to 89% indicating that the auto-tuner is able to get close to the desired charge regime consistently. We show the confusion matrix of the evaluation of the model in Fig. 7. The entries on the diagonal in the confusion matrix correspond to successful runs, whereas off-diagonal entries represent unsuccessful runs. In particular, one can use off-diagonal entries to identify how exactly each of the erroneous outcomes were misclassified. The off-diagonal entries indicate that most errors occur due to the presence of charge transitions that the algorithm did not recognize in the data. The reverse effect, i.e. identifying a transition that is not physically present in the system, almost never occurs. Thus, we conclude that a weak signal-to-noise ratio in the measurements is the main reason for false classifications. The accuracies, 99% and 96% respectively, in identifying the individual transitions are high in the context of neural network classifiers [36, 37]. The total success rate of the auto-tuner is lower than the individual success rate of the neural networks due to cumulative error from the repeated application of the neural networks.

VI. CONCLUSION AND OUTLOOK

In this work we implemented and experimentally tested a machine learning assisted auto-tuner that sets the plunger gate voltages to reach any charge configuration of a DQD. We verified that the accuracy of the resulting algorithm persists when testing it on a different DQD than for which the machine learning models

Confusion Matrix - Complete Tuning Runs

(1,0)	0	3	0	0	0	0	0	0	0	0	
(1,1)	0	28	2	3	0	0	0	0	0	0	
(1,2)	0	9	24	0	2	0	0	0	0	1	
(2,1)	0	1	0	22	1	0	0	0	0	0	
(2,2)	0	1	0	7	17	0	0	0	0	0	
(0,2)	0	0	2	0	0	0	0	0	0	0	
(2,0)	0	0	0	1	0	0	0	0	0	0	
(2,3)	0	0	0	0	10	0	0	0	0	0	
(3,2)	0	0	0	1	0	0	0	0	0	0	
(1,3)	0	1	8	0	2	0	0	0	0	0	
(2,4)	0	0	0	1	6	0	0	0	0	0	
(1,4)	0	0	2	0	0	0	0	0	0	0	
(1,5)	0	1	0	0	0	0	0	0	0	0	
(2,5)	0	0	0	1	1	0	0	0	0	0	
		(1,0)	(1,1)	(1,2)	(2,1)	(2,2)	(0,2)	(2,0)	(2,3)	(3,2)	(1,3)

Predicted Charge Occupation

FIG. 7. Confusion matrix indicating the outcomes of the test runs of the auto tuner. The rows indicate the actual charge occupation after terminating the algorithm and the column indicates the auto tuners prediction. Two runs are omitted, since their charge occupation could not be determined.

were trained on. In our experiments we reached a success rate of around 60%. The primary error source is identified as a weak signal-to-noise ratio. We believe this could in principle be alleviated by performing more finely grained measurements for the subsets of the charge stability diagram and, thus, training the convolutional neural networks on higher resolution images. Another suitable strategy is to implement more targeted sampling of the charge stability diagram [22]. Currently, we perform homogeneous steps in voltages at all positions of the chosen patch. Measuring more densely around the places of the diagram where the local standard deviation of the data is maximal would lead to better resolution of the transition lines and might increase the accuracy of the algorithm as well. Further improvements might arise from including simulated data into the training set [34].

Generally, neural networks are very good at performing fast and efficient classification, but it is extremely difficult to arrive at 100% accuracy on any training set of practical significance. Thus, the accuracy of individual tuning steps will always have a finite success rate when implemented with a neural network architecture and these finite rates will accumulate if many steps are needed to reach the final state of tuning. These types of auto-tuners may therefore still require some form of human input. Alternatively, additional algorithms that consider the full problem instance, rather than only individual steps, could serve as a better approach.

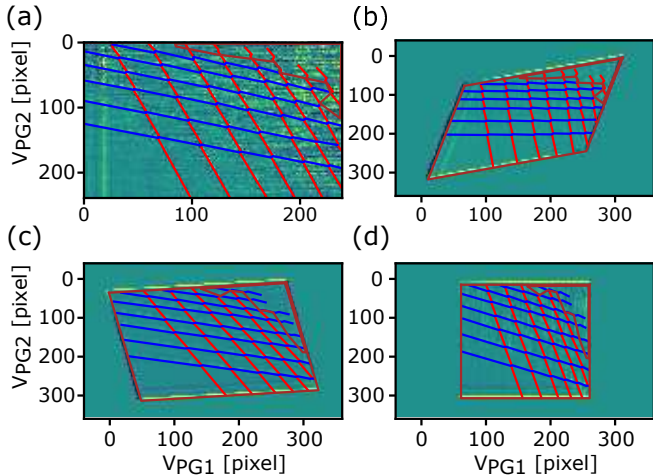


FIG. 8. (a) Charge stability diagram with indicated charge transitions. Blue lines correspond to charge transition lines of QD2 and red lines to charge transitions of QD1. In the area enclosed by the brown line no charge transition lines could be recognized. (b) - (d) Three different augmentations with randomly chosen transformations of (a).

Parameter	Value
Dropout 1	0.05
Conv. Layer 1	$(4, 4) \times 48$
Activation 1	ReLU
Dropout 2	0.05
Conv. Layer 2	$(3, 3) \times 12$
Activation 2	ReLU
Dropout 3	0.4
Dense Layer	50
Activation	sigmoid
Outputs	2
Activation	softmax
Loss	categorical crossentropy
Optimizer	adam
Batch size	128
Learning rate	0.001
Epochs	8
Class weights	True

TABLE I. Relevant parameters used to create the neural network used to determine charge transition lines in the coarse patches are shown.

ACKNOWLEDGEMENTS

We gratefully acknowledge financial support from the Swiss National Science Foundation, the NCCR QSIT. This work has received funding from the European Research Council under grant agreement no. 771503. We thank Sebastian D. Huber and Klaus Ensslin for fruitful discussions.

Parameter	Value
Dropout 1	0.2
Conv. Layer 1	$(6, 6) \times 72$
Activation 1	ReLU
Dropout 2	0.1
Conv. Layer 2	$(3, 3) \times 24$
Activation 2	ReLU
Dropout 3	0.2
Conv. Layer 3	$(2, 3) \times 12$
Activation 3	ReLU
Dropout 4	0
Dense Layer	50
Activation	sigmoid
Outputs	3×4
Activation	softmax
Loss	categorical crossentropy
Optimizer	adam
Batch size	128
Learning rate	0.001
Epochs	8
Class weights	False

TABLE II. Relevant parameters used to create the neural network that recognizes individual charge transition between the corners of the high resolution patches are shown.

Class	precision	recall	f1	support
occupied	0.996	0.986	0.991	2063
empty	0.975	0.993	0.984	1089
Micro Avg.	0.989	0.989	0.989	3152

TABLE III. Classification scores for the neural network used to determine charge transition lines in the coarse patches. The numbers are obtained from the evaluation data-set containing 3152 data-points. The micro average corresponds to the overall accuracy, i.e. the fraction of data points that are correctly classified.

Appendix A: Measurements and Data Processing

All measurements were recorded in a commercially available dilution refrigerator with a base temperature of 12mK. The electronic temperature is $132\text{mK} \pm 9\text{mK}$.

In Fig. 8 we show a charge stability diagram (a) and three of its random augmentations (b) - (d). The charge stability diagrams have a resolution of 1mV and size $241\text{mV} \times 241\text{mV}$. Subsequently, approximately 300 fine patches are drawn from each of the augmented charge stability diagrams (including their original).

The individual augmentation transformations are: (i) rotation of the whole charge stability diagram, (ii) rotation of 45 degrees followed by scaling the diagram in the PG1 and/or PG2 direction followed by a rotation of -45 degrees, (iii) scaling the PG1 axis, (iv) scaling the PG2 axis and (v) flip of the PG1 and PG2 axes. Flipping the axes simulates measurements for which the plunger gate voltages are swept in reverse order. For all charge stability diagrams, the final augmentation sequence consists

Class	precision	recall	f1	support
(0, 0)	0.97	0.97	0.98	1202
(0, 1)	0.96	0.95	0.95	643
(1, 0)	0.97	0.93	0.95	157
(1, 1)	0.83	0.83	0.83	52
Micro Avg.	0.96	0.96	0.96	2054

TABLE IV. Classification scores for the classification of the charge transitions occurring between lower left and top left corner of the high resolution patches. The numbers are obtained from the evaluation data set containing 2054 data points. The micro average corresponds to the overall accuracy, i.e. the fraction of data points that are correctly classified.

of randomly picking one of all transformations with random transformation parameters as e.g. rotation angle or scaling factor.

After augmentations of all charge stability diagrams are performed, the patches are drawn. In order to distribute the patches equally over the charge stability diagram, but still preserve randomness, we decided to draw the patches of size 28×28 px, where the grid points are randomly shifted by up to five pixels in each direction.

Each of the patches is processed separately. In the first processing step, the data is rescaled such that the variance equals to one. Secondly, we construct the charge

stability diagrams by evaluating the derivative of the measured current I_{QPC} according to the formula

$$\frac{\partial I_{QPC}}{\partial V_{PG}} = \frac{1}{2} \left(\frac{\partial I_{QPC}}{\partial V_{PG1}} + \frac{\partial I_{QPC}}{\partial V_{PG2}} \right). \quad (A1)$$

Subsequently, we remove far outlying measurement points based on a fixed standard deviation criterion.

Appendix B: Machine Learning Models

Both machine learning models are constructed in Python using the high-level Tensorflow API Keras [38]. All hyper-parameters which define the architectures are shown in Tab. II and in Tab. I. Tables III, IV, V and VI show the performance of the two neural networks on the evaluation data set. The scores we show are the following: recall which is calculated as the number of elements that were evaluated correctly by the network divided by the number of true positives, precision which is the number of elements that were evaluated as positive divided by total number of samples and f1 which is harmonic mean between the recall and precision [39]. The accuracy score, which is the fraction of correctly classified data-points, is given by the micro average of the above scores.

-
- [1] WIL Lawrie, HGJ Eenink, NW Hendrickx, JM Boter, L Petit, SV Amitonov, M Lodari, B Paquelet Wuetz, C Volk, S Philips, *et al.*, “Quantum dot arrays in silicon and germanium,” arXiv preprint arXiv:1909.06575 (2019).
- [2] Philip Krantz, Morten Kjaergaard, Fei Yan, Terry P Orlando, Simon Gustavsson, and William D Oliver, “A quantum engineer’s guide to superconducting qubits,” *Applied Physics Reviews* **6**, 021318 (2019).
- [3] Elsa Prada, Pablo San-Jose, Michiel WA de Moor, Attila Geresdi, Eduardo JH Lee, Jelena Klinovaja, Daniel Loss, Jesper Nygård, Ramón Aguado, and Leo P Kouwenhoven, “From andreev to majorana bound states in hybrid superconductor-semiconductor nanowires,” arXiv preprint arXiv:1911.04512 (2019).
- [4] Romana Schirhagl, Kevin Chang, Michael Loretz, and Christian L. Degen, “Nitrogen-vacancy centers in diamond: Nanoscale sensors for physics and biology,” *Annual Review of Physical Chemistry* **65**, 83–105 (2014), pMID: 24274702.
- [5] CE Bradley, J Randall, MH Abobeih, RC Berrevoets, MJ Degen, MA Bakker, M Markham, DJ Twitchen, and TH Taminau, “A 10-qubit solid-state spin register with quantum memory up to one minute,” arXiv preprint arXiv:1905.02094 (2019).
- [6] Morten Kjaergaard, Mollie E. Schwartz, Jochen Braumüller, Philip Krantz, Joel I-Jan Wang, Simon Gustavsson, and William D. Oliver, “Superconducting qubits: Current state of play,” (2019), arXiv:1905.13641.

Class	precision	recall	f1	support
(0, 0)	0.97	0.98	0.97	632
(0, 1)	0.95	0.96	0.95	517
(1, 0)	0.96	0.96	0.96	500
(1, 1)	0.95	0.93	0.94	405
Micro Avg.	0.96	0.96	0.96	2054

TABLE V. Classification scores for the classification of the charge transitions occurring between lower left and top right corner of the high resolution patches. The numbers are obtained from the evaluation data set containing 2054 data-points. The micro average corresponds to the overall accuracy, i.e. the fraction of data points that are correctly classified.

- [7] Frank Arute, Kunal Arya, Ryan Babbush, Dave Bacon, Joseph C Bardin, Rami Barends, Rupak Biswas, Sergio Boixo, Fernando GSL Brandao, David A Buell, *et al.*, “Quantum supremacy using a programmable superconducting processor,” *Nature* **574**, 505–510 (2019).
- [8] Marius Eich, Riccardo Pisoni, Hiske Overweg, Annika Kurzmann, Yongjin Lee, Peter Rickhaus, Thomas Ihn, Klaus Ensslin, František Herman, Manfred Sigrist, *et al.*, “Spin and valley states in gate-defined bilayer graphene quantum dots,” *Physical Review X* **8**, 031023 (2018).
- [9] Fabrizio Nichele, Asbjørn CC Drachmann, Alexander M Whiticar, Eoin CT O’Farrell, Henri J Suominen, Antonio Fornieri, Tian Wang, Geoffrey C Gardner, Candice

Class	precision	recall	f1	support
(0, 0)	0.98	0.99	0.98	1193
(0, 1)	0.90	0.87	0.89	151
(1, 0)	0.98	0.97	0.97	643
(1, 1)	0.84	0.78	0.81	63
Micro Avg.	0.97	0.97	0.97	2054

TABLE VI. Classification scores for the classification of the charge transitions occurring between lower left and lower right corner of the high resolution patches. The numbers are obtained from the evaluation data set containing 2054 data-points. The micro average corresponds to the overall accuracy, i.e. the fraction of data points that are correctly classified.

- Thomas, Anthony T Hatke, *et al.*, “Scaling of majorana zero-bias conductance peaks,” *Physical review letters* **119**, 136803 (2017).
- [10] R. M. Lutchyn, E. P. A. M. Bakkers, L. P. Kouwenhoven, P. Krogstrup, C. M. Marcus, and Y. Oreg, “Majorana zero modes in superconductor-semiconductor heterostructures,” *Nature Reviews Materials* **3**, 52–68 (2018).
- [11] E. Kawakami, P. Scarlino, D. R. Ward, F. R. Braakman, D. E. Savage, M. G. Lagally, Mark Friesen, S. N. Coppersmith, M. A. Eriksson, and L. M. K. Vandersypen, “Electrical control of a long-lived spin qubit in a si/sige quantum dot,” *Nature Nanotechnology* **9**, 666–670 (2014).
- [12] K. C. Nowack, F. H. L. Koppens, Yu. V. Nazarov, and L. M. K. Vandersypen, “Coherent control of a single electron spin with electric fields,” *Science* **318**, 1430–1433 (2007).
- [13] Y. He, S. K. Gorman, D. Keith, L. Kranz, J. G. Keizer, and M. Y. Simmons, “A two-qubit gate between phosphorus donor electrons in silicon,” *Nature* **571**, 371–375 (2019).
- [14] D. J. van Woerkom, P. Scarlino, J. H. Ungerer, C. Müller, J. V. Koski, A. J. Landig, C. Reichl, W. Wegscheider, T. Ihn, K. Ensslin, and A. Wallraff, “Microwave photon-mediated interactions between semiconductor qubits,” *Phys. Rev. X* **8**, 041018 (2018).
- [15] P. Scarlino, D. J. van Woerkom, U. C. Mendes, J. V. Koski, A. J. Landig, C. K. Andersen, S. Gasparinetti, C. Reichl, W. Wegscheider, K. Ensslin, T. Ihn, A. Blais, and A. Wallraff, “Coherent microwave-photon-mediated coupling between a semiconductor and a superconducting qubit,” *Nature Communications* **10**, 3011 (2019).
- [16] A. J. Landig, J. V. Koski, P. Scarlino, C. Müller, J. C. Abadillo-Uriel, B. Kratochwil, C. Reichl, W. Wegscheider, S. N. Coppersmith, Mark Friesen, A. Wallraff, T. Ihn, and K. Ensslin, “Virtual-photon-mediated spin-qubit-transmon coupling,” *Nature Communications* **10**, 5037 (2019).
- [17] F. Borjans, X. G. Croot, X. Mi, M. J. Gullans, and J. R. Petta, “Long-range microwave mediated interactions between electron spins,” (2019), arXiv:1905.00776.
- [18] Julian Kelly, Peter O’Malley, Matthew Neeley, Hartmut Neven, and John M Martinis, “Physical qubit calibration on a directed acyclic graph,” arXiv preprint arXiv:1803.03226 (2018).
- [19] Eliska Greplova, Edward A Laird, G Andrew D Briggs, and Klaus Mølmer, “Conditioned spin and charge dynamics of a single-electron quantum dot,” *Physical Review A* **96**, 052104 (2017).
- [20] CJ Van Diepen, Pieter T Eendebak, Bruno T Buijten-dorp, Uditendu Mukhopadhyay, Takafumi Fujita, Christian Reichl, Werner Wegscheider, and Lieven MK Vandersypen, “Automated tuning of inter-dot tunnel coupling in double quantum dots,” *Applied Physics Letters* **113**, 033101 (2018).
- [21] Steffen J Glaser, Ugo Boscain, Tommaso Calarco, Christiane P Koch, Walter Köckenberger, Ronnie Kosloff, Ilya Kuprov, Burkhard Luy, Sophie Schirmer, Thomas Schulte-Herbrüggen, *et al.*, “Training schrödinger’s cat: quantum optimal control,” *The European Physical Journal D* **69**, 279 (2015).
- [22] D. T. Lennon, H. Moon, L. C. Camenzind, Liuqi Yu, D. M. Zumbühl, G. A. D. Briggs, M. A. Osborne, E. A. Laird, and N. Ares, “Efficiently measuring a quantum device using machine learning,” *npj Quantum Information* **5**, 1–8 (2019).
- [23] Eliska Greplova, Christian Kraglund Andersen, and Klaus Mølmer, “Quantum parameter estimation with a neural network,” arXiv preprint arXiv:1711.05238 (2017).
- [24] Julian D. Teske, Simon Sebastian Humpohl, René Otten, Patrick Bethke, Pascal Cerfontaine, Jonas Dedden, Arne Ludwig, Andreas D. Wieck, and Hendrik Bluhm, “A machine learning approach for automated fine-tuning of semiconductor spin qubits,” *Applied Physics Letters* **114**, 133102 (2019).
- [25] Easwar Magesan, Jay M Gambetta, Antonio D Córcoles, and Jerry M Chow, “Machine learning for discriminating quantum measurement trajectories and improving readout,” *Physical review letters* **114**, 200501 (2015).
- [26] J. Darulová, S.J. Pauka, N. Wiebe, K. W. Chan, M.C. Cassidy, and M. Troyer, “Autonomous tuning and charge state detection of gate defined quantum dots,” arXiv preprint arXiv:1911.10709 (2019).
- [27] Sandesh S. Kalantre, Justyna P. Zwolak, Stephen Ragole, Xingyao Wu, Neil M. Zimmerman, M. D. Stewart, and Jacob M. Taylor, “Machine learning techniques for state recognition and auto-tuning in quantum dots,” *npj Quantum Information* **5**, 1–10 (2019).
- [28] Eliska Greplova, Carolin Gold, Benedikt Kratochwil, Tim Davatz, Riccardo Pisoni, Annika Kurzmann, Peter Rickhaus, Mark H Fischer, Thomas Ihn, and Sebastian Huber, “Fully automated identification of 2d material samples,” arXiv preprint arXiv:1911.00066 (2019).
- [29] Gang Cao, Hai-Ou Li, Guo-Dong Yu, Bao-Chuan Wang, Bao-Bao Chen, Xiang-Xiang Song, Ming Xiao, Guang-Can Guo, Hong-Wen Jiang, Xuedong Hu, and Guo-Ping Guo, “Tunable hybrid qubit in a GaAs double quantum dot,” *Physical Review Letters* **116** (2016).
- [30] Zhan Shi, C. B. Simmons, J. R. Prance, John King Gamble, Teck Seng Koh, Yun-Pil Shim, Xuedong Hu, D. E. Savage, M. G. Lagally, M. A. Eriksson, Mark Friesen, and S. N. Coppersmith, “Fast hybrid silicon double-quantum-dot qubit,” *Physical Review Letters* **108** (2012).
- [31] J. Medford, J. Beil, J. M. Taylor, E. I. Rashba, H. Lu, A. C. Gossard, and C. M. Marcus, “Quantum-dot-based resonant exchange qubit,” *Physical Review Letters* **111** (2013).
- [32] A. J. Landig, J. V. Koski, P. Scarlino, U. C. Mendes, A. Blais, C. Reichl, W. Wegscheider,

- A. Wallraff, K. Ensslin, and T. Ihn, “Coherent spin–photon coupling using a resonant exchange qubit,” *Nature* **560**, 179–184 (2018).
- [33] Maximilian Russ, J. R. Petta, and Guido Burkard, “Quadrupolar exchange-only spin qubit,” *Phys. Rev. Lett.* **121**, 177701 (2018).
- [34] Justyna P Zwolak, Thomas McJunkin, Sandesh S Kalantre, JP Dodson, ER MacQuarrie, DE Savage, MG Lagally, SN Coppersmith, Mark A Eriksson, and Jacob M Taylor, “Auto-tuning of double dot devices in situ with machine learning,” arXiv preprint arXiv:1909.08030 (2019).
- [35] W. G. van der Wiel, S. De Franceschi, J. M. Elzerman, T. Fujisawa, S. Tarucha, and L. P. Kouwenhoven, “Electron transport through double quantum dots,” *Rev. Mod. Phys.* **75**, 1–22 (2002).
- [36] Han Xiao, Kashif Rasul, and Roland Vollgraf, “Fashion-mnist: a novel image dataset for benchmarking machine learning algorithms,” arXiv preprint arXiv:1708.07747 (2017).
- [37] Li Deng, “The mnist database of handwritten digit images for machine learning research [best of the web],” *IEEE Signal Processing Magazine* **29**, 141–142 (2012).
- [38] François Chollet *et al.*, “Keras,” <https://github.com/fchollet/keras> (2015).
- [39] Aurélien Géron, *Hands-on machine learning with Scikit-Learn and TensorFlow: concepts, tools, and techniques to build intelligent systems* (“O’Reilly Media, Inc.”, 2017).